Experimentally uncertainty quantification in numerical and analytical beam models

P. Langer[1]; K. Sepahvand[2]; M. Krause[3]; S. Marburg[2]

[1,2] Universität der Bundeswehr Munich, 85579 Neubiberg, Germany

[3] Isko-engineers AG, 80807 Munich, Germany

ABSTRACT

In modern industrial processes such as developing new products, virtual prototyping is state of the art method to ensure short design cycles while dealing with low cost pressure. In order to meet these criteria, efficient and reliable simulations must be available. Numerical methods, especially the Finite Element Method (FEM) are commonly used in various industrial fields e.g. the automotive sector, aircraft design and ship construction. The scope of this paper is to enhance the reliability of numerical models utilizing FEM when considering uncertain parameters of the underlying structure. Such parameters can be system related, i.e. geometry, material behavior, boundary conditions and mesh density as well as general assumptions in the process of modeling. Two well-known beam theories, i. e. Euler-Bernoulli and Timoshenko theory, have been utilized. At FE level, various elements available for modeling of beam structures in ABAQUS have been compared and evaluated. Experimental modal analysis have been performed on beam specimen to validate the results from analytical and FE models due to parameter uncertainties. A comparison between the numerical and analytical simulations with experiments reveal the element types with minimum deviation with regard to parameter uncertainties. Having sufficient knowledge of the dynamic behavior of simple beam samples, the complexity will be increased. This investigation developed instructions on how detailed a numerical model must be built to get satisfactory results.

Keywords: Uncertainty quantification, FE modeling, beam structures, experimental modal analysis

1. INTRODUCTION

A model is an abstraction of reality in which many assumptions are made. It is not possible to evaluate correct results without knowing the underlying assumptions (1, 2). For this reason it is important to find exactly the right model that is the most suitable for the conceptual formulation. In the formation of the mathematical models the minimum description length principle (MDL) proposed by Rissanen (3) is one useful approach to finding the shortest description of the data and the model itself. Ross Quinlan and Rives provide a good description of MDL principle in (4). The method, however, does not include the estimation of errors in the results.

Model building and simulation are becoming increasingly important in engineering. In simulation phase, the Finite Element Method (FEM) is manly used to construct a numerical model. Within the past decade increasing in computer capability, FEM has become highly important in model formation for engineers. Additionally, in industry, FEM has crucial importance for reducing the number of experimental examinations. The major issue is that every FEM model possess some degree of uncertainty due to topological and material parameters, initial and boundary conditions, forcing term, etc. The results from FEM models are trustable if they are validated with experimental or results from available analytical models. When comparing the models, however, uncertainties must be taken into account. General recommendations regarding model uncertainties are given in (5) that are important for model formation and in the development process. A powerful tool in numerical simulation of engineering problems involve uncertainty is the stochastic finite element method (SFEM), which is an extension of deterministic FEM in random framework (6). The application of the method on various practical engineering problems including uncertainty has been studied in many works, cf. (7, 8, 9, 10, 11, 12) This paper present a comparison of numerical, analytical models and the experimental results for beam structures involving material and parameter uncertainties. The results have been studied for various quadratic tetrahedral and hexahedral elements types with different number of elements to realize the model uncertainties.

[1] Patrick.Langer@unibw.de

The one–dimensional solution obtained by Euler–Bernoulli and Timoshenko was used for the analyses in this study. The physical model for experimental results depends on the precision of the measuring equipment and the apparatus used to perform an experiment. The considered uncertainties include material and shape, while model uncertainties include boundary conditions, model assumptions, model depth and level of detail. The model depth, is, by definition, the formation of elements, and the level of detail is the number of elements. The investigation includes a study of the model depth and the level of detail in which the FE model is verified for the analytical solution is first described, this is followed by verification for an overkill calculation. The physical, numerical and analytical models will be compared using the best regular mesh determined. Later, when the models get more complexity, it is not possible to mesh the whole geometrical irregularities. Therefore, the influence of distortion in numerical mesh is investigated. A recommendation is given since a virtual image for exactly one simple real shape can be made. Abaqus/CAE was used as a pre- and postprocessor for this task. In the experimental modal analysis, the free–free beam specimens were contact free excited by a periodic chirp signal by means of loudspeakers. The resonance frequencies of the first 3 bending modes were measured with a Laser–Doppler–Vibrometer.
The remainder of the paper is organized as follows. Section 2 reviews the investigated FEM, analytical and experimental models. The numerical simulations of the method illustrate in section 3. Section 4 discusses the conclusions.

2. MODEL DESCRIPTION

In this section, we discuss the details of FEM, analytical and experimental models considered in the investigation.

2.1 FEM models

For this study the model was created in Abaqus/CAE and submitted to the Abaqus/standard implicit solver. Various types of elements in the mesh module can be selected in the Abaqus element library. Table 1 shows the elements that were available for the study.

Table 1 – Element description from elements, that were selected in the Abaqus element library for the study (13).

Name	Nodes	Basis function	General marks
C3D20	20	quadratic	three dimensional quadratic brick
C3D20R	20	quadratic	three dimensional quadratic brick with reduced integration
C3D20H	20	quadratic	three dimensional quadratic brick with linear pressure formulation
C3D10	10	quadratic	three dimensional tetrahedron
C3D10M	10	quadratic	three dimensional tetrahedron with hourglass control
C3D10I	10	quadratic	three dimensional tetrahedron with improved stress visualization
C3D10H	10	quadratic	three dimensional tetrahedron with linear pressure formulation
C3D8	8	linear	three dimensional linear brick

All elements have a quadratic formulation function because linear formulation functions stiffen the structure at bending. The highest possible precision of the models are investigated and compared in this study.

2.2 Analytical Models

The analytical model is based on two well–known Euler–Bernoulli and Timoshenko beam theories. The Euler–Bernoulli beam theory assumes no shear deflection and rotary inertia. For this reason the Timoshenko theory is formulated to cover this drawbacks. This theory also includes assumptions. One of these is that, the shear stress distribution across the cross section is assumed to be constant and linear. It is also assumed that the cross–sectional area is symmetric so that the neutral and centroidal axes coincide. A comprehensive study on various beam theories is given in (14). Although many high–order beam theories are available, they will be disregarded here. The analytical solutions lead to one–dimensional equations, which does not represent many physical effects on the structure. That must be clear for the results.

2.3 Physical Models and Experiments

The physical model uses experimental modal analysis in which beam samples were suspended from two elastic strings and activated acoustically with a periodic chirp signal by a loudspeaker. A chirp is a signal in which frequency increases or decreases over time. Measurements are carried out in an anechoic chamber to

avoid the influence of acoustic reflections from the walls. The microphone measures effective sound pressure generated by the loudspeaker to find the input value for the FRF. The deflection shape was measured by a Laser–Doppler–Vibrometer in front of the beam shape. Figure 1 shows the measuring setup seen from the Vibrometer: microphone (1), the loudspeaker (2), beam shape (3), elastic strings (4) and anechoic chamber (5). The eigenfrequencies and the associated bending modes were found numerically using ME'scope.

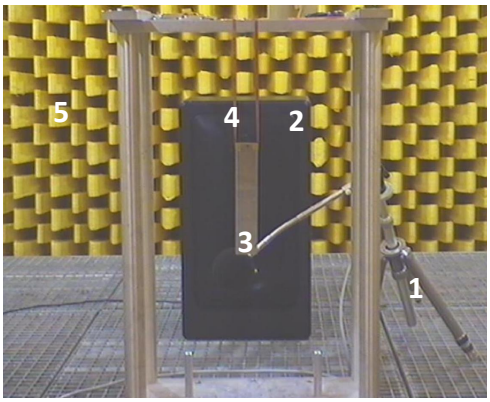

Figure 1 – Experimental setup of beam samples, suspended by means of two elastic strings and excitatory acoustically with a periodic chirp signal by a loudspeaker.

3. RESULTS

In this section the study results are presented. The beam samples are made of steel and aluminum and homogeneous and elastic material properties were assumed. The nominal values of uncertain material and geometrical parameters of 10 beam samples are given in Table 2. The deviation of the density for the 10

Table 2 – The nominal values of uncertain geometrical and material parameters.

Parameter	Steel	Aluminum
Length, L [mm]	200	200
Width, B [mm]	40	40
Thickness, H [mm]	4	4
Density [kgm^{-3}]	7817	2663
Young's modulus [Gpa]	211	72
Poisson's ratio [-]	0.30	0.34

steel samples is 13.43 kgm^{-3} and for the 10 aluminum samples 0.38 kgm^{-3}. The other material uncertain parameters for each individual sample are shown in Fig. 2. The line with crosses represents the uncertainty for each measurement. The standard deviation consists of a complex mathematical evaluation of the ten samples. The shape uncertain parameters are the length L of the beam, the width B and the thickness H. The upper and lower limits of this geometrical parameters are taken into account. A search is performed for the most roughly regular mesh FE model with the lowest deviations from the analytical models. One model of the forty FEM models are considered in which the element edge length and layer number were varied. The results have been studied for various quadratic tetrahedral and hexahedral elements types with different number of elements to realize the model uncertainties. The models meshed with a regular mesh without distorted elements. Sample FEM mesh is shown in Fig. 3 with two layers and an element edge length of 5 mm. Two models from each sample were made in this way. Teh deviation error is based on the analytical model defined by

$$\varepsilon_A = \left(\frac{f_N}{f_A} - 1 \right) \times 100, \tag{1}$$

in which ε_A is the relative deviation, f_A and f_N are analytical and numerical bending eigenfrequency, respectively. The calculation plan is shown in Fig. 4. Each of three Abaqus elements, C3D20, C3D20H and C3D20R are calculated with one, two and three layers with the corresponding element edge lengths. With two layers, an element edge length of 1 mm and a C3D20 element type, the error reaches a minimum. For all models,

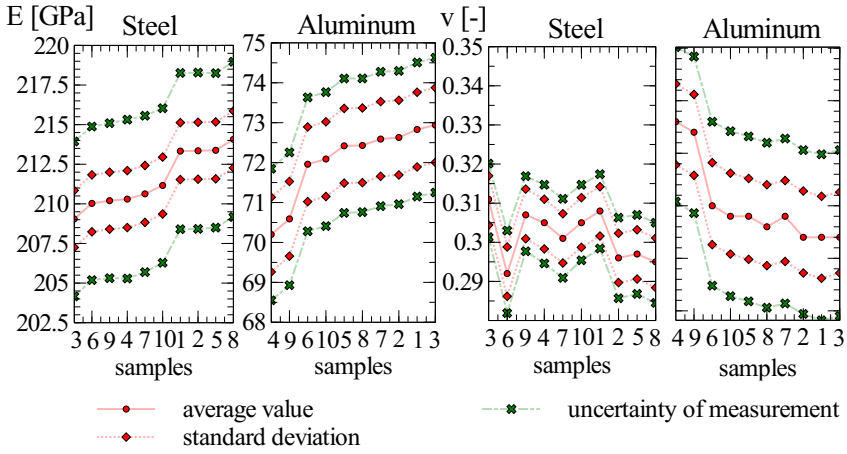

Figure 2 – Variation of material parameters and their deviation,
E: Young's modulus, ν: Poisson's ratio

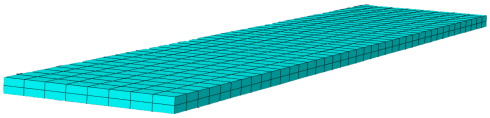

Figure 3 – Sample FE model for steel beams

except for the framed element types shown, the value of the convergence remains constant in the precision investigated. The increase in the element number means only a longer computing time without substantial changes to result value. The same procedure was used for tetrahedron elements. The calculation scheme is shown in Fig. 5. For tetrahedron elements, the C3D10M has the minimal averaged deviation with 3 layers and an element edge length of 1 mm compared to the analytical model. As opposed to the hexahedron elements, no trend can be recognized at a degree of cross–linking shape that the solution converges to a value.

The most efficient FE model for the two element types could be identified. Table 3 shows the relative deviations of the first three bending eigenfrequencies in comparison with the analytical results defined using Eq. (1). The deviation at the first bending mode is very low and increases insignificantly for the following two. The degree of cross–linking determined was compared with an overkill solution to analyze the value of the convergence changes strongly at very many more elements. The number of elements in the overkill solution is a factor of 10 for the hexahedral elements and 28 for tetrahedral elements. The value of the relative deviations from the overkill solution is smaller than 0.04%. This means that there are no differences in the value of convergence compared to a much finer cross–linked regular mesh.

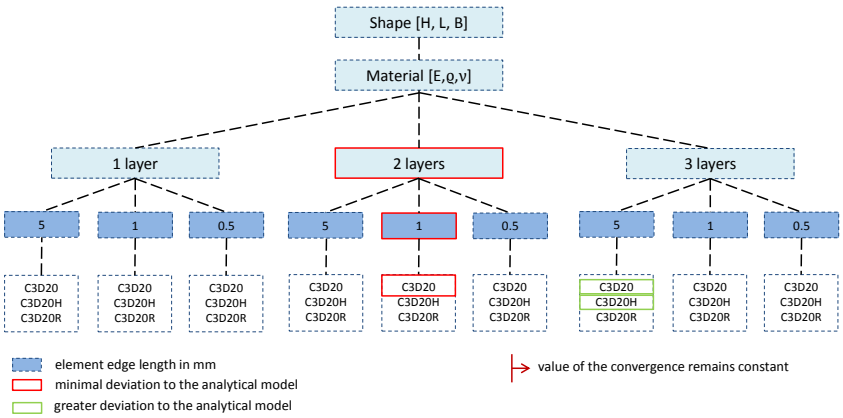

Figure 4 – The calculation plan 1. Each of three elements, C3D20, C3D20H and C3D20R are calculated with one, two and three layers with the corresponding element edge lengths of 0.5, 1 and 5 mm.

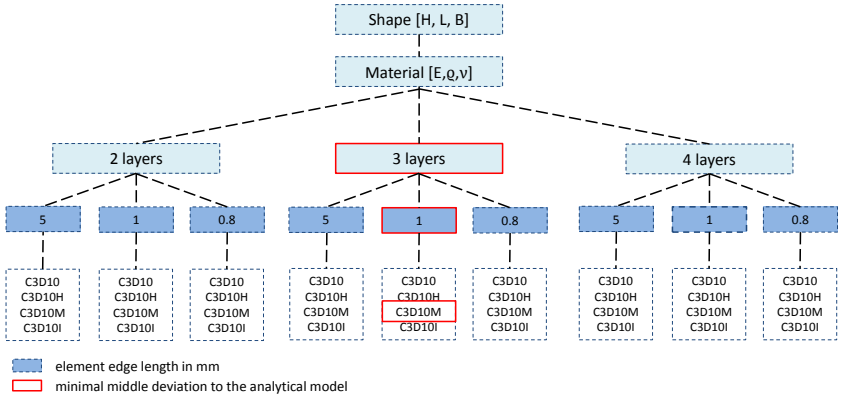

Figure 5 – The calculation plan 2. Each of three elements, C3D10, C3D10H, C3D10M and C3D10I are calculated with two, three and four layers with the corresponding element edge lengths of 0.8, 1 and 5 mm.

Table 3 – Deviation of the first three bending eigenfrequencies calculated from FEM model in comparison with analytical results, ε_h : relative deviation of hexahedron elements, ε_t : relative deviation of tetrahedron elements.

Frequencies	f_1	f_2	f_3
ε_h	0.14	0.4	0.4
ε_t	0.03	0.27	0.39

3.1 Model Uncertainty

The uncertainty in the investigated models possesses different composition. Aleatory and epistemic uncertainties are defined. Aleatory uncertainties are taken into account in each of three model types. Boundary conditions, material and shape are included. The epistemic uncertainties must be considered in detail for every model type. In the FE model the discretization and the weak formulation to Galerkin are included. In analytical models, the assumptions described in section 2.2 were made. Measurements include errors in reading, measurement setup and the inherent stress condition of the samples. Figure 6–(a) and 6–(b) show the eigenfrequencies of the first three bending modes of steel and aluminum samples. The numerical models are meshed with the most roughly mesh were we found at the beginning in section 3. A tube–shaped identified upper and lower limits that surround the mean value indicate the complete deviation. Agreement for the first eigenfrequency was very high. In addition, it was found to be physically correct that the physical model is limited by virtual models. The first eigenfrequencies for the 10 samples of steel are in an uncertain frequency range of 30 Hz. For the second and third eigenfrequencies this range increased considerably. The uncertain frequency range of the samples of aluminum were very low about the first three bending modes. The following applies for aluminum and steel samples. The Euler–Bernoulli model and the FE model show a high level of agreement. This is not the case for Timoshenko models even though shear deflection was considered. This did become relevant until the third eigenfrequency. With the exception of the Timoshenko models, the models displayed a high level of agreement also here. The election of element formulation in this approach is less important to determine the eigenfrequencies. Models with C3D20 and C3D10M element types have a great agreement with such simple structures. Uncertainties that occur due to model assumptions or different element formulation (model depth) do not simply have to be written in values. This partitioning of the uncertainties, arithmetically averaged over 10 samples is given in 7. The bar chart shows the relative deviation in the bending modes compared to an ideal model for the first three eigenfrequencies. This base model is chosen in different ways. The individual bar sections must be read in a stratified manner and not from the zero point of the ordinate. For the calculation of uncertainties regarding the model assumptions proposed by Timoshenko and Euler–Bernoulli, the FE model is used as a virtually ideal model. For element formulation the physical model is the ideal model and the FE model for material and shape uncertainties. The deviations in the model assumptions according to Euler–Bernoulli are constant within the first three bending modes. For the Timoshenko model these increase strongly with a higher bending mode and are much higher than for Euler–Bernoulli. The element formulation with elements C3D20 has a lower deviation compared to the physical model than with the C3D10M tetrahedron elements. The uncertainties of material parameters have the highest influence on the complete relative deviation. This includes the density ρ, the Young's modulus E and the Poisson's ratio ν. At the shape parameters the thickness H, length L and width B of the beam

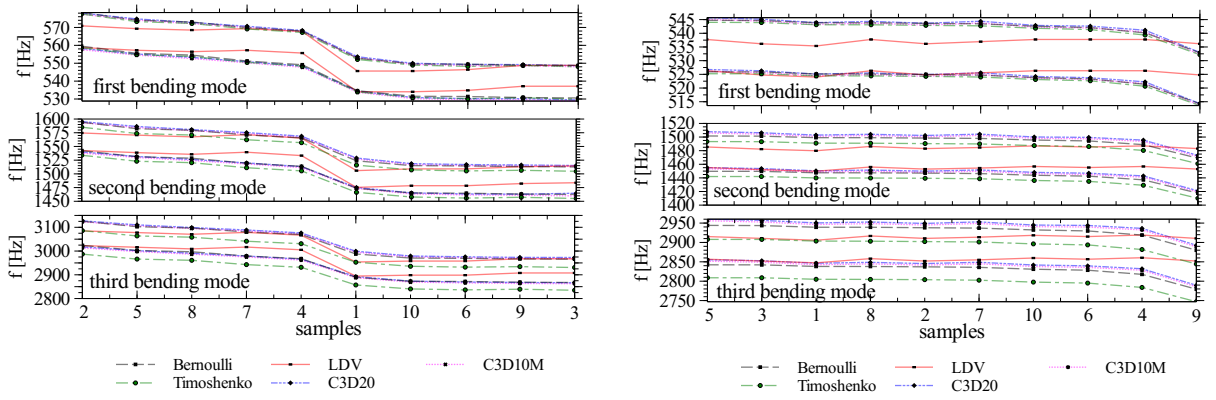

Figure 6 – The first three eigenfrequencies of the bending modes with uncertainties. (a): steel samples, (b): aluminum samples

were analyzed. The relative deviation in material parameters and shape parameters is constant for the first three eigenfrequencies of the bending modes. With the exception of an analytical Timoshenko beam, the total deviation remains constant as the bending modes increase.

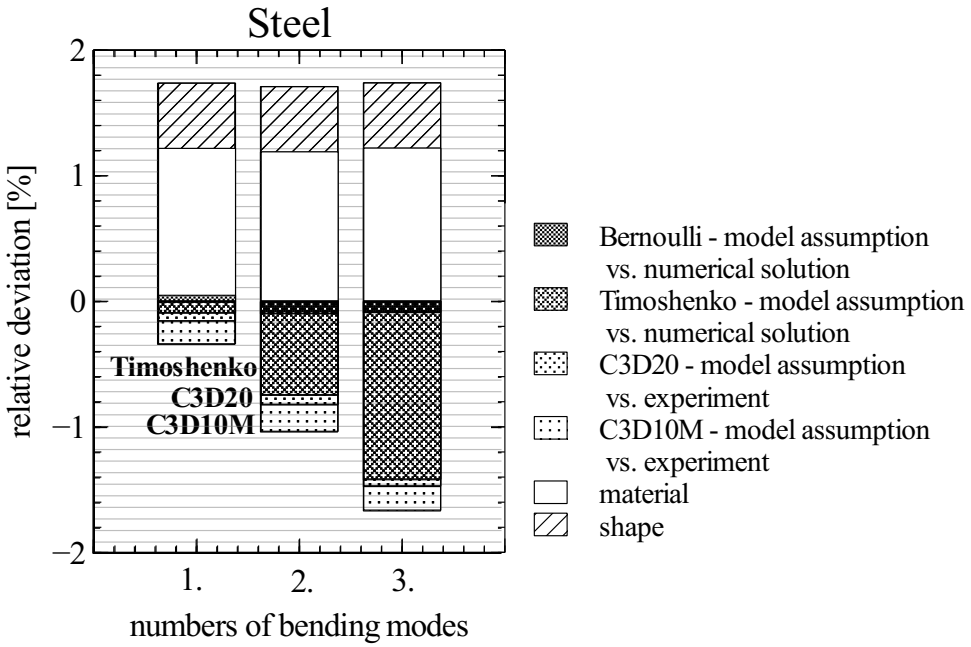

Figure 7 – Individual uncertainties about 10 samples – arithmetic mean values – stacked.

3.2 Influence of distorted elements

The purpose of this section is to analyze the influence of distorted mesh elements on the total numerical errors. For simple beam structures, distorted mesh have been analysed on the total numerical errors. For the mesh of simple numerical models of beam structures, distorted elements could be avoided. For more complex structures that can not be excluded, therefore it is important for the next steps of the work to know the influence of distorted elements exactly to the numerical solution. Lee and Bathe (15) classified the distortion of two–dimensional elements in six different categories, which are shown in figure 8. In Fig. 8–(a), a square element with evenly spaced nodes is shown as the undistorted element. In Fig. 8–(b), the distortion is the cause of very high aspect ratio in direction of the two coordinates r and s. Lee and Bathe defined in figure 8–(c) a state of distortion due to the unequal position of the nodes on the element edges. The displacement of the element node to a parallelogram is shown in figure 8–(d). In figure 8–(e) the element is distorted due to a curved edge. Figure 8–(f) shows a distorted element by the large and small angle between two element edges with a common node. As Lee and Bathe described, The same principle as described by Lee and Bathe is used

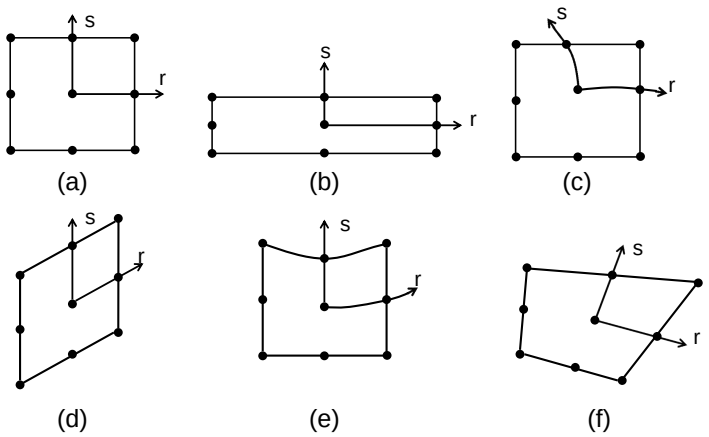

Figure 8 – Classification of two-dimensional element distortion (15)

in Abaqus/CAE mesh verification feature to check the quality of mesh elements. For each critical/distorted element either a warning or an error message is reported. In the former case, despite the warning message, Abaqus solver is capable of handling the model. When the criteria exceed a certain level, however, an error message is displayed and Abaqus solver cannot be started. The verification part of the mesh in Abaqus checks the quality of the elements and gives for each critical element a warning or an error. In the first case, the model for the solver of Abaqus remains solvable. If these criteria are injured too much, Abaqus issues an error message and the solver can not be started.
In Abaqus, the surface is differentiated in form and size criteria. Two sub-criteria are used for this study: The angle criterion and a geometric deviation factor. The former considers the angle between two element edges that converge in a node. For angles larger than 10 degrees, no warning or error messages are issued. The geometric deviation factor is defined by

$$\frac{d_{\text{element}}}{l_{\text{element}}} < 0.2, \tag{2}$$

in which d_{element} is the distance between the the distorted and undistorted states of the element edge and l_{element} is the length of this element edge. The limits for each criterion can be changed in Abaqus manually.

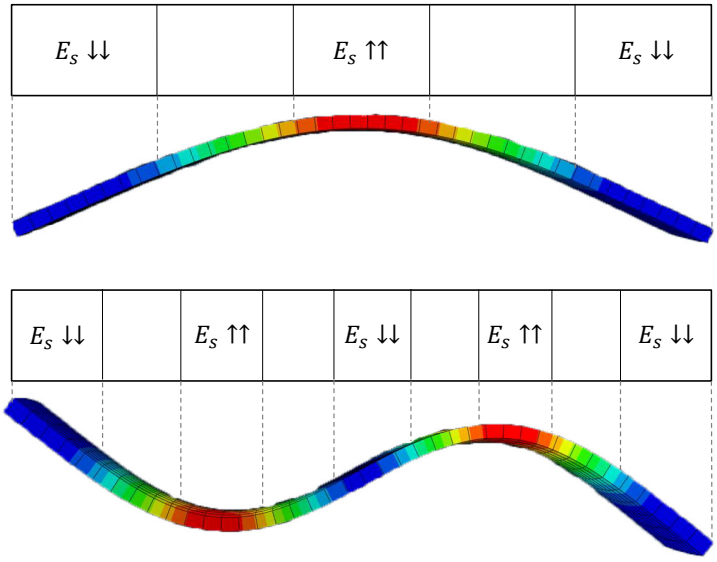

Figure 9 – Total elastic strain energy E_s for the first and second bending mode; mesh: 1 layer, 5 mm element edge length; top: first bending mode; bottom: second bending mode

Figure 9 shows the principle approach of the study. The structure is divided into high and low total elastic strain energy, E_s. If the change in the number of elements in each field exceeds a certain percentage of the total number of elements, Abaqus issues a warning message, although the model remains solvable. The results of these models have been compared to a reference model, without distorted elements. By dividing certain areas of minimum and maximum deformation energy, a statement regarding the position of distorted elements and their impact can be made to calculate the eigenfrequencies of these bending modes. The numerical models are meshed with quadratic hexahedral elements C3D20, one layer and 5 mm element edge length or with three dimensional 8 node linear elements C3D8. In Figure 10, solutions for the first and second eigenfrequency of the bending modes are shown. The largest relative deviation for a model with distorted mesh elements from an undistorted (reference) model, $\varepsilon_{\max}$ is defined as

$$\varepsilon_{\max} = \left(\frac{f_d}{f_r} - 1 \right) \times 100, \tag{3}$$

where f_d and f_r are respectively the obtained eigenfrequencies of a bending mode for a numerical model with and without distortion. Here, the distorted elements account for 10% of the total number of the mesh elements. Figure 10–(a) shows the results for the model with hexahedral mesh elements (C3D20) for the first and second bending modes. In areas with low elastic strain energy, the relative deviation is almost independent of the number of distorted elements in the region and is less than 0.03%. In contrast, at regions with high elastic strain energy, the relative deviation increases with the number of distorted elements and reaches values of 0.62% and 0.5% for the first and second eigenfrequencies, respectively.

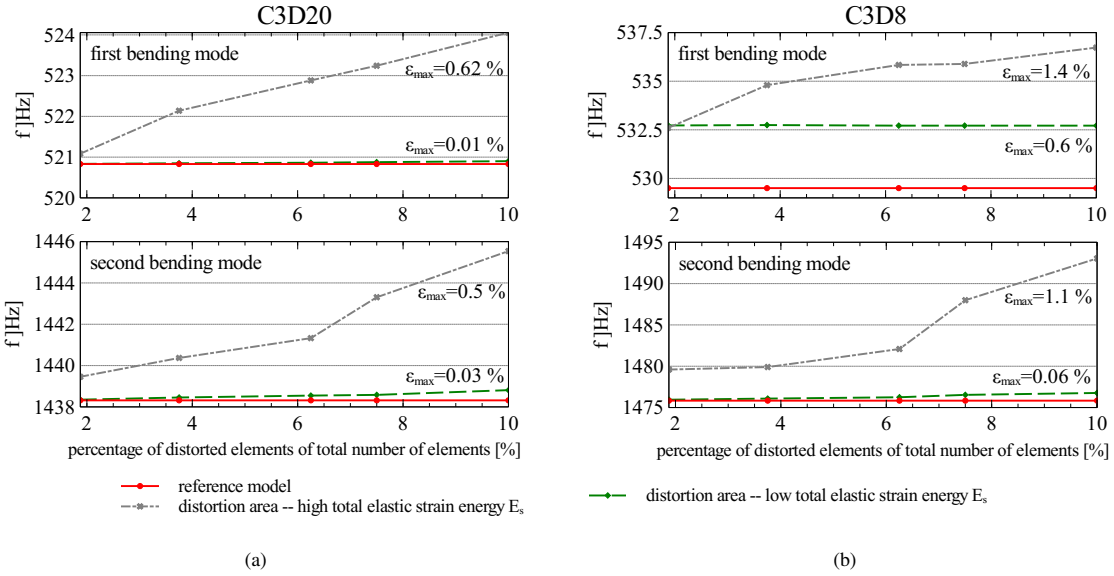

Figure 10 – Results are compared to a reference case without any distortion. $\varepsilon_{\max}$: maximum relative deviation with 10% distorted elements compared to a reference model without distortion. (a): mesh element typ C3D20; (b): linear elementtyp C3D8

The relative deviation for the models with linear mesh elements C3D8 is shown in figure 10–(b). The relative deviation for the first eigenfrequency at low total elastic strain energy region is shown to be constant and equal to 0.6% everywhere, where as for the second bending mode, this value slightly goes up with the number of distorted elements. Again, at regions with high total elastic strain energy, the relative deviation becomes higher with increasing number of distorted elements. Values are 1.4% and 1.1% for the first and second bending modes, respectively. In the second eigenfrequency is here the maximum deviation at 0.06% to the reference model. Here, the relative deviation becomes higher with increasing number of distorted elements in regions of high total elastic strain energy and reaches a maximum for the first and second eigenfrequency of 1.4% and 1.1%. Results indicate that the quality of a numerical mesh depends on two important features: 1. the total number of distorted mesh elements 2. the concentration region of the distorted elements considering the deformation in the area. The relative deviations $\varepsilon_{\max}$ for models with distorted elements to the reference seems relatively small with < 1.5%. However, one must note that the investigated beam geometry very simple. It might be reasonably assumed that increases the influence of distorted elements on the eigenfrequencies of bending modes with increasing complexity of the structure.

3.3 Comparison to experimental models

In this section the FE models for which the most efficient mesh for hexahedral and tetrahedral elements were found, the Euler–Bernoulli beam and Timoshenko beam are compared with reality, that is results from experimental modal analysis. Material and shape parameters are mean average values. Figure 11 shows the relative deviation, ε_P , from experimental (physical) model defined as

$$\varepsilon_P = \left(\frac{f_{n/a}}{f_e} - 1 \right) \times 100, \tag{4}$$

where $f_{n/a}$ and f_e are the numerical/analytical and experimental bending eigenfrequencies. The results for 10 models made of steel over the abscissa are connected by lines and colored areas. An area that signifies a complete deviation for more than 10 samples results for every model type. The surface sections must be read in a stratified manner and not from the zero point of the ordinate. The FE model with the hexahedral element formulation C3D20 has the lowest relative deviation from the physical model. The deviation decreases even more with increasingly higher bending modes. The arithmetic mean values of relative deviation for more than 10 samples and the first three eigenfrequencies of bending modes is -0.06%, -0.07% and -0.05%. For the FE model with the C3D10M element type the following deviations were determined: -0.18%, -0.21% and -0.19%. The FE solution for a model with hexahedron elements, an element edge length of 1 mm and a layer number of 2 are thus closer to physical model. This can be clearly seen by the surface representation in Figure 11. The Euler–Bernoulli model still show a good agreement compared the physical model. With increasingly higher bending mode the Timoshenko model has the largest deviations from the physical model. Figure 11 shows the same results, but for the 10 models made of aluminium. Comparing FE models with the C3D20

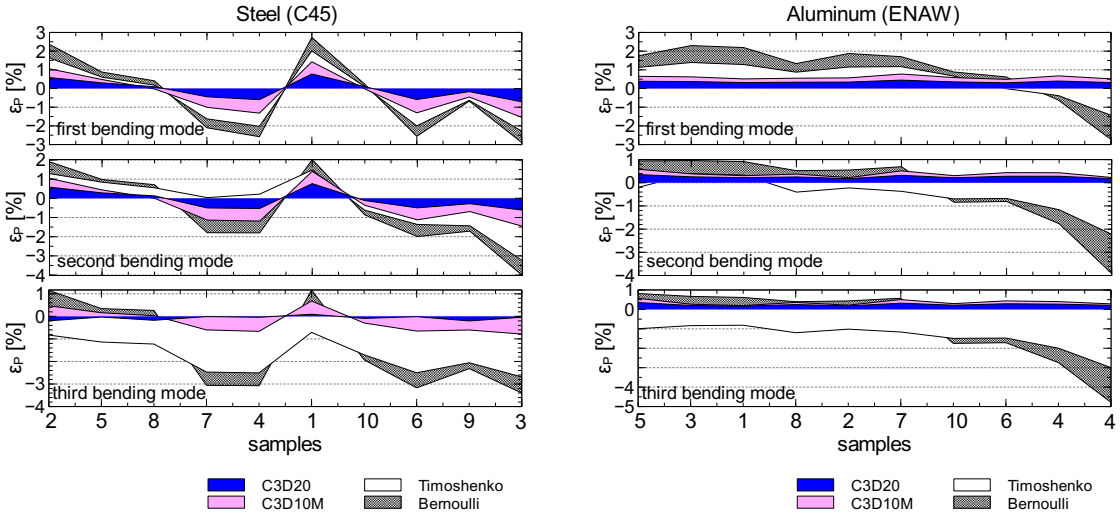

(a) (b)

Figure 11 – Relative deviation about 10 samples to physical model - stacked area. (a): steel samples, (b): aluminum samples

and C3D10M element formulations reveals interesting results. Unlike the steel samples the model is closer to the physical model with the tetrahedron mesh. The arithmetic mean values of relative deviation for more than 10 samples for the first three eigenfrequencies of bending modes is 0.25%, 0.14% and 0.13%. For the FE model with the C3D20 element type, the deviations were 0.38%, 0.27% and 0.26%. Euler–Bernoulli and Timoshenko beams behave in a similar fashion as in the case of steel samples.

4. CONCLUSIONS

This paper has attempted to provide a recommendation regarding the level of discretization in FE models with simple structures at which results converge. It provides the engineer with certainty regarding the sufficient number degrees of freedom in simple beam structures. An element type for this case was proposed. It was shown that uncertainties regarding material and shape parameters always have a considerable influence on the eigenfrequencies of bending modes. The uncertainties for the model assumptions according Timoshenko were the only ones that had a significant increase with the bending modes. Numerical, physical and analytical models have a high level agreement up to the third eigenfrequency of the bending modes. It is shown analytical models, this does not converge absolutely to a better result despite a high–order beam theory. In these examinations the simpler Euler–Bernoulli model has a higher agreement with the physical and FE models. The comparison to physical models shows that the FE models have the lowest deviation to the reality. For steel samples the most accurate element type is C3D20. Otherwise, for aluminum samples the tetrahedron elements C3D10M. The influence of distorted mesh elements on the total numerical errors has been investigated. Results indicated that the quality of a numerical mesh depends on the total number of distorted mesh elements and the concentration region of the distorted elements considering the deformation in the area. It is demonstrated that mesh areas with low elastic strain energy, the relative deviation is almost independent of the number of distorted elements in the region. This is in contrast to regions with high elastic strain energy where the relative deviation increases with the number of distorted elements.

REFERENCES

1. Balci O. Credibility Assessment of Simulation Results: The State of the Art. In: Eastern Simulation Conferences. Orlando, Fla.; 1987. p. 1–8.
2. Sevgi L. Modeling and Simulation Concepts in Engineering Education: Virtual Tools. Turkish Journal of Electrical Engineering and Computer Sciences. 2006;14(1):113–12.
3. Rissanen J. An Introduction to the MDL Principle. Helsinki Institute for Information Technology; Tampere and Helsinki Universities of Technology, Finland, and University of London, England;.
4. Quinlan JR, Rives RL. Inferring Decision Trees Unsing the Minimum Description Length Principle. Massachusetts: Academic Press; 1989.
5. Sargent G. Verification and Validation of Simulation Models. In: Winter Simulation Conferences. Orlando; 2005. p. 53–59.
6. Stefanou G. The stochastic finite element method: Past, present and future. Computer Methods in Applied Mechanics and Engineering. 2009;198(9–12):1031–1051.
7. Li R, Ghanem R. Adaptive polynomial chaos expansions applied to statistics of extremes in nonlinear random vibration. Probabilistic Engineering Mechanics. 1998;13(2):125–136.
8. Lucor D, Su CH, Karniadakis GE. Generalized polynomial chaos and random oscillators. International Journal for Numerical Methods in Engineering. 2004;60(3):571–596.
9. Soize C. A comprehensive overview of a non–parametric probabilistic approach of model uncertainties for predictive models in structural dynamics. Journal of Sound and Vibration. 2005;288(3):623–652.
10. Sepahvand K, Marburg S, Hardtke HJ. Stochastic free vibration of orthotropic plates using generalized polynomial chaos expansion. Journal of Sound and Vibration. 2012;331(1):167–179.
11. Marburg S, Beer HJ, Gier J, Hardtke HJ. Experimental verification of structural–acoustic modelling and design optimization. Journal of Sound and Vibration. 2002;252(4):591–615.
12. Sephavand K, Marburg S. On construction of uncertain material parameter using generalized polynomial chaos expansion from experimental data. In: IUTAM Symposium on Multiscale Problems in Stochastic Mechanics. Karlsruhe; 2012. p. 4–17.
13. Abaqus User and Theory Manual 6.10-3;.
14. Han SM, Benaroya H, Wei T. Dynamics of transversely vibrating beams using four engineering theories. Journal of Sound and Vibration. 1999;225(5):935 – 988.
15. Lee NS, Bathe KJ. Effects of Element distortions on the performance of isoparametric elements. International Journal for numerical Methods in engineering. 1993;36:3553–3576.